

Development of T_N Quadrature Sets and HEART Solution Method
 for Calculating Radiative Heat Transfer

C. P. Thurgood¹, H. A. Becker¹, E. W. Grandmaison¹
 A. Pollard², P. Rubini^{1,2}, A. Sobiesiak^{1,2}

¹Department of Chemical Engineering

²Department of Mechanical Engineering
 Queen's University, Kingston, Ontario.

Abstract: - The accuracy of the Discrete Ordinate Method is improved for non-scattering radiant heat transfer in infinite ducts. This is accomplished by using a new family of quadrature sets (designated as T_N) that can be extended to an indefinite number of rays. Second, the equation of transfer is solved using a new scheme called HEART. Using the same grid, the HEART scheme is capable of greater accuracy than a solution technique based on central differencing.

Introduction

In many industrial furnaces, the dominant mode of heat transfer is thermal radiation. The procedure to compute radiant heat transfer forms an important module of the models of these furnaces. The purpose of the module is to generate the radiative heat flux in the gas and on surfaces given the temperature field. The procedure usually employs a grey-gas mixture model to predict gas emission. The procedure needs to be accurate yet economical in execution time and computer memory. It should be applicable for a range of absorption coefficients and capable of handling irregular furnace geometry. It should also be able to handle obstructions within the furnace.

Assuming a gas fired furnace, the following common assumptions are made to simplify the computational task without significant loss of accuracy:

1. scattering is negligible
2. the surfaces of the furnace can be approximated as a grey Lambert surfaces
3. gas emission is modelled using a grey gas mixture

These assumptions lead to the following set of equations that permit the calculation of the radiant heat transfer for a typical component of the grey gas mixture. The equation of transfer for a grey gas:

$$\mu \frac{\partial I}{\partial x} + \frac{\partial I}{\partial y} + \xi \frac{\partial I}{\partial z} = KI_{b,gas} - KI \quad (1)$$

and the boundary condition:

$$I_{surface}(\vec{\Omega}) = \epsilon I_{b,surface} + \frac{\rho}{\pi} \int_{\vec{n} \cdot \vec{\Omega}' < 0} |\vec{n} \cdot \vec{\Omega}'| I_{surface}(\vec{\Omega}') d\Omega' \quad (2)$$

for $\vec{n} \cdot \vec{\Omega} > 0$

The radiant heat flux at a point in the gas is calculated from:

$$\nabla \cdot \vec{q} = 4\pi K I_{b,gas} - K \int I(\vec{\Omega}) d\Omega \quad (3)$$

In the above equations, \vec{n} is an inward normal at the surface, $\vec{\Omega}$ represents an incoming or outgoing direction at the surface and $d\Omega$ is a differential solid angle. The blackbody intensity (I_b) of the gas and surface is given by $\sigma T^4/\pi$.

The direction cosines (μ, η, ξ) in the equation of transfer (1) determine the direction $\vec{\Omega}$ of travel of the ray. They assume any value between -1 to +1 subject to the condition:

$$\mu^2 + \eta^2 + \xi^2 = 1 \quad (4)$$

Many existing procedures are not suitable for the computational task at hand. The ZONE method (Hottel and Sarofim, (1967)) is not attractive since large grids would require a long execution time to compute exchange areas for an irregularly shaped enclosure and matrix inversion. The Spherical Harmonic method is not suitable as the optical depth of the control volume must be ≥ 0.5 , Viskanta and Monguc, (1987). The flux methods are too inaccurate, Siddall and Selcuk (1979), Selcuk (1985, 1988), and Lockwood and Shah (1978). Raithby and Chui (1989) presented a new method that looks promising but needs further testing.

The Discrete Ordinate Method (DOM) has recently been investigated by Fiveland (1984, 1988), Hydo and Truelove (1977), Truelove (1987, 1988), and Jamaluddin and Smith (1988) and shown to yield adequate accuracy in comparison to benchmark calculations for a wide range of absorption coefficients.

There are however a number of deficiencies in DOM that need to be overcome to increase its accuracy. The solution technique of Fiveland (1984, 1988), and Hydo and Truelove (1977) uses central differencing to extrapolate the intensity across a control volume. As a result, the Solution technique can:

1. generate non-physical oscillations in the intensity field, Fiveland (1988)
2. produce negative intensities on the face of a control volume

Fiveland (1988) sets negative surface intensities to zero and carries on with the calculation. This yields a computationally efficient algorithm that gives good results. Other schemes are available for dealing with negative intensities (Hyde and Truelove (1977), Jamaluddin and Smith (1988)) that are more computationally demanding yet do not yield clearly superior results. The combination of central differencing and "set-negative-

intensities-to-zero" is herein labelled as Fiveland's scheme.

The last limitation of DOM is that there are only three quadrature sets, denoted by S_4 , S_6 , and S_8 (Fiveland, (1988) and Truelove, (1987)), recommended for practical computation. This limits the accuracy of the method and hinders tests for grid independence.

This paper describes a new algorithm for solving the equation of transfer, equation (1). The Heuristic Embedding Algorithm for Ray Tracing, or HEART scheme, will be presented for two dimensional infinite duct radiation. The HEART scheme is coupled with a new family of quadrature sets that can be extended to indefinite number of rays. Designated as T_N , the quadrature sets satisfy the symmetry requirements developed by Lathrop and Carlson (1968) to avoid bias in numerical results induced by the labelling of the co-ordinate axes.

First, the HEART scheme is presented and then compared to Fiveland's scheme using a standard test problem. The derivation of the T_N quadrature sets is then reviewed. The last section compares numerical results from the the HEART scheme and T_N quadrature sets with benchmark calculations for two dimensional infinite duct radiation problems.

Review of Discrete Ordinates Method

The angular integrals appearing in the boundary condition (2) and formula for the heat flux in the gas (3) are estimated by numerical quadrature. The boundary condition becomes:

$$I_{surface}(\vec{\Omega}) = \epsilon I_{b,surface} + \frac{\rho}{n} \sum_{\vec{n} \cdot \vec{\Omega}_i < 0} w_i |\vec{n} \cdot \vec{\Omega}_i| I_{surface}(\vec{\Omega}_i) \quad (5)$$

while the formula for the heat flux in the gas reads:

$$\nabla \cdot \vec{q} = 4\pi K I_{b,gas} - K \bar{I} \quad (6)$$

where w_i is the weight corresponding to the direction $\vec{\Omega}_i$. In two dimensional Cartesian geometry, a direction $\vec{\Omega}_i$ has the direction cosines (μ_i, η_i) which satisfy the inequality:

$$\mu_i^2 + \eta_i^2 \leq 1 \quad (7)$$

The equation of transfer is solved in the directions specified by the quadrature set. In two dimensional geometry, it reads:

$$\mu_i \frac{\partial I}{\partial x} + \eta_i \frac{\partial I}{\partial y} = K I_{b,gas} - K I \quad (8)$$

Fiveland (1984, 1988) and Truelove (1977) present solution techniques for the equation of transfer based upon upwind or central differencing.

Description of HEART Scheme

The HEART scheme is based upon multi-grid techniques combined with ray tracing to solve the equation of transfer. It will be assumed that the coarse grid is rectangular but otherwise arbitrary. Each coarse control volume is subdivided with a fine grid. The intensity field is computed on the fine grid and the results are assembled to form a representative value for the intensity field on the coarse grid. The fine grid consists of a number of parallel "channels". The direction of the channels is parallel to the direction of travel of the intensity field. Figure 1 demonstrates a typical coarse control volume overlaid with a

fine grid viewed in the XY plane. Note that the fine grid need not be uniform.

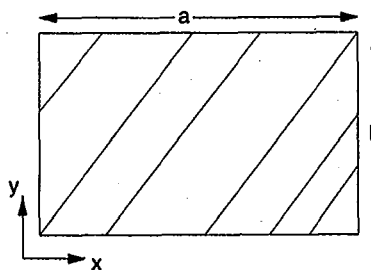


Figure 1. Coarse Control Volume Overlaid with Fine Control Volumes

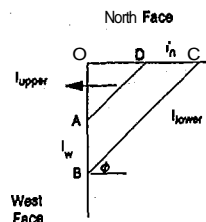


Figure 2. Typical Channel of the Fine Grid

To illustrate the derivation of the equations for HEART, consider a typical fine control volume as shown in figure 2. Denote the lengths of the sides of the quadrilateral ABCD by l_w , l_n , l_{upper} and l_{lower} . Integration of (8) over a fine control volume and application of Gauss' Theorem yields:

$$-\mu l_w I_w + \eta l_n I_n = K I_{b,gas} A - K I_p A \quad (9)$$

The area A of the quadrilateral is:

$$(l_{lower}^2 - l_{upper}^2) \cos(\phi) \sin(\phi) / 2 \quad (10)$$

Geometry yields:

$$l_w = (l_{lower} - l_{upper}) \sin(\phi) \quad (11)$$

$$l_n = (l_{lower} + l_{upper}) \cos(\phi) \quad (12)$$

Equations (10), (11) and (12) are substituted into Eqn. (9) along with the relations:

$$\mu = \sin(\theta) \cos(\phi) \quad (13)$$

$$\eta = \sin(\theta) \sin(\phi) \quad (14)$$

$$\xi = \cos(\theta) \quad (15)$$

After some manipulation,

$$I_{b,gas} - I_p = (I_n - I_w) / K t \quad (16)$$

where

$$t = (l_{lower} + l_{upper}) / 2 \sin(\theta) \quad (17)$$

The distance t is the distance along the ray that connects the midpoints of the sides AB and CD of the quadrilateral. The distance ($t \sin \theta$) is the length of the projection of the ray on the XY plane.

In order to compute I_p , an additional relationship is required. This additional relationship is obtained from the analytic solution to the equation of transfer. Along the direction of travel, the solution to the equation of transfer is:

$$I(s) = I_0 e^{-Ks} + I_{b,gas}(1 - e^{-Ks}) \quad (18)$$

where s is the co-ordinate along the ray and I_0 is the intensity at $s = 0$. We may consider that I_w and I_n are located at the respective midpoints of their face. Application of the above formula yields:

$$I_n = I_w e^{-Kt} + I_{b,gas}(1 - e^{-Kt}) \quad (19)$$

Substitution into (16) yields the following explicit formula for calculating I_p :

$$I_p = I_w \left\{ \frac{1 - e^{-Kt}}{Kt} \right\} + I_{b,gas} \left\{ 1 - \frac{1 - e^{-Kt}}{Kt} \right\} \quad (20)$$

Given I_w , equations (19) and (20) allow I_n and I_p to be computed explicitly. Similar formula can be derived for other quadrilaterals. The formulae can be summarized as:

$$I_{leaving} = I_{entering} e^{-Kt} + I_{b,gas}(1 - e^{-Kt}) \quad (21)$$

$$I_p = I_{entering} \left\{ \frac{1 - e^{-Kt}}{Kt} \right\} + I_{b,gas} \left\{ 1 - \frac{1 - e^{-Kt}}{Kt} \right\} \quad (22)$$

where the distance t is given in Table 1 and depends on the combination of the entering and leaving face.

Entering face	Leaving face	Distance t
West	North	Equation (17)
West	East	a/μ
South	North	$b/7?$
South	East	Equation (17)

Table 1: Effective path lengths for computing leaving and average intensity for quadrilaterals; a,b: see Fig. 1.

For the channels that are triangular in shape (eg. triangle OAD, figure 2), the above formulae are correct if I_{upper} (or I_{lower} depending on the location) is set to zero.

The volume averaged intensity for the coarse control volume is obtained by noting:

$$A_{coarse} I_{coarse} = \int_{A_{coarse}} I dA = \sum_{A_{fine}} I_{p,fine} dA = \sum_{A_{fine}} I_{p,fine} A_{fine} \quad (23)$$

This leads to:

$$I_{p,coarse} = \frac{\sum I_{p,fine} A_{fine}}{A_{coarse}} \quad (24)$$

The volume averaged intensity for the coarse control volume is the area weighted summation of the fine grid intensity divided by the area of the coarse control volume.

The final step in the solution technique is mapping the leaving intensity from a coarse control volume to the entering intensity for an adjacent control volume. The difficulty is that the leaving faces of the channels do not coincide with the entering

faces of the channels of the adjacent control volumes. The entering intensities will be computed by ensuring that the flux of radiant energy entering a channel is equal to the flux of radiant energy impinging upon it from the leaving faces of the channels of the adjacent control volume. This leads immediately to:

$$I_{entering}^{leaving} = \sum I_{leaving}^{overlapping} \quad (25)$$

where the summation applies to the leaving surfaces that have some portion of their area overlapping the area of the entering surface.

The generation of the intensity field for the coarse grid follows the same sequence of steps as in Fiveland's (1988) scheme. Assume that the direction cosines, μ and η , are both positive. The boundary intensities on the west and south boundaries of the computational domain become the entering intensities for coarse control volumes adjacent to the boundaries. The entering intensities for the channels within a coarse control volume are all equal. The leaving intensities and average channel intensity are computed using equations (21) and (22). The average intensity for the coarse control volume is calculated using (24). The entering intensities for the adjacent (north and east) control volumes are computed from the leaving intensities using equation (25). The coarse grid intensity field is generated by a point by point computation with all quantities being explicitly calculated. At the north and east boundaries, an average surface intensity is computed as the summation of the length weighted leaving intensities divided by the length of the face of the coarse control volume. The average surface intensity is used in the boundary equation (2).

Inspection of equations (21) and (20) shows that the proposed scheme ensures that the leaving and nodal intensity is always non-negative and bounded. Equation (21) also guarantees that the intensity field is non-oscillatory.

The HEART scheme is more computationally demanding than central differencing due to the need to calculate an exponential for each channel and interpolate to find entering intensities from the leaving intensities. In this work, uniform coarse grids will be used. The interpolation factors and coefficient in equations (21), (20), (23) and (24) are stored to eliminate repetitive computation.

The fine control volumes, for this work, are obtained by dividing the west and south faces of the coarse control volumes into equal segments. The subdivision is indicated in the notation, for example, 2+4. This indicates that the west face is subdivided into two equal segments, while the south face is subdivided into four equal segments.

The HEART scheme has some similarities to the step characteristic method (Lathrop (1969), Larsen (1982)) as the surface of a control volume is subdivided into segments. In the step characteristic method, the intensities on the segments are combined to form an average intensity applicable over the entire face. This average intensity is transmitted to the adjacent control volume. In contrast, the HEART scheme transmits the intensities on the segments to the adjacent control volume. The HEART scheme tracks the variation of the intensity over the face of a control volume leading to increased accuracy.

Comparison of HEART Scheme and Fiveland's Scheme

The two schemes are compared on the following test problem: a square duct contains a grey gas with a uniform emittance of

one. The **emittance** of the west and south walls are respectively 1 and 0. The intensity field is computed for rays that travel at some angle (θ) with respect to the south boundary.

The ray through the origin divides the square into two regions. Above this ray, the intensity field is one as the gas is in equilibrium with the west wall. Below the ray, the intensity field starts at zero at the south wall and increases to one according to the formula: $1 - \exp(-Kt)$, where t is the distance along the ray.

Along the ray starting at the origin, there is a discontinuity in the intensity field. The magnitude of the discontinuity decreases for non-zero absorption coefficient but it persists for the case of zero absorption coefficient. The intensity at the origin is defined to be one-half, the average of the surface intensity on either side of the discontinuity.

In order to quantify the comparison of the two methods, the average absolute deviation (or global error) is computed for each scheme for varied grid and angle. It is computed by summing the absolute difference between the numerical intensity and the exact point intensity over all control volumes and dividing by the number of control volumes.

Figure 3 presents the average absolute deviation for Fiveland's scheme as a function of varied directions and grid refinements. The error is zero for angles of 0, 90 and 45 degrees. The zero error occurs at angles of 0 and 90 degrees since the problem reduces to the one-dimensional transport of a constant radiation field where central differencing gives exact results.

The zero error at 45 degrees occurs since the discontinuity falls onto the diagonal of the control volume. The extrapolation from west to east and south to north is symmetrical and yields a nodal value of one-half, one for the north face and zero for the east face. As the exact intensity is defined to be one-half, the numerical error is zero. Since the intensity on the north face is precisely one, oscillations above the discontinuity are suppressed. This yields an intensity field of one everywhere above the discontinuity. Similarly, the zero intensity on the east face ensures that the intensity field is zero everywhere below the discontinuity. The global error is then zero.

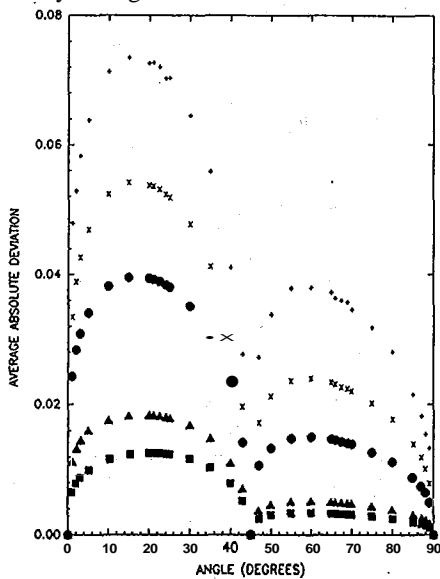


FIGURE 3. GLOBAL ERROR (SINGLE PRECISION) VERSUS ANGLE FOR FIVELAND'S SCHEME. ABSORPTION CO-EFFICIENT = 0.
 • 25 X 25 GRID; a 50 X 50 GRID; • 100 X 100 GRID;
 A 500 X 500 GRID; • 1000 X 1000 GRID.

The global error for angles between 45 and 90 degrees is substantially less than that for angles less than 45 degrees. The region above the discontinuity is reduced in size so that the numerical error generated by the oscillations is reduced.

Figures 4 and 5 present the global error for the HEART scheme for zero absorption coefficient using 1+1 and 5+5 channels. Both curves show zero error at 0, 45 and 90 degrees. The zero error at these angles occurs because the interpolation between adjacent control volume faces is exact (i.e. there is no mismatch between entering and leaving channels adjacent coarse control volumes) and the interpolation (20) is exact for zero absorption coefficient.

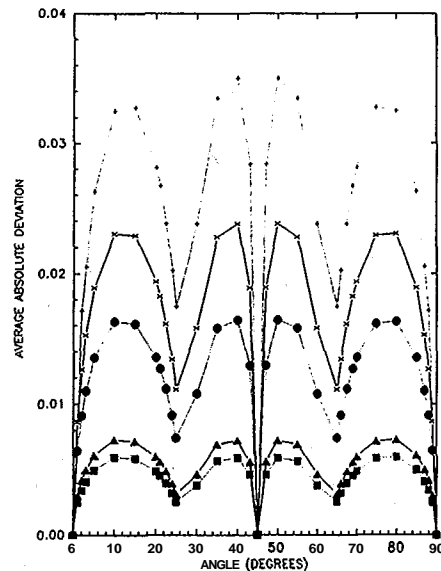


FIGURE 4. GLOBAL ERROR (SINGLE PRECISION) VERSUS ANGLE FOR HEART SCHEME, 1+1. ABSORPTION CO-EFFICIENT = 0.
 • 25 X 25 GRID; x 50 X 50 GRID; • 100 X 100 GRID;
 A 500 X 500 GRID; • 750 X 750 GRID.

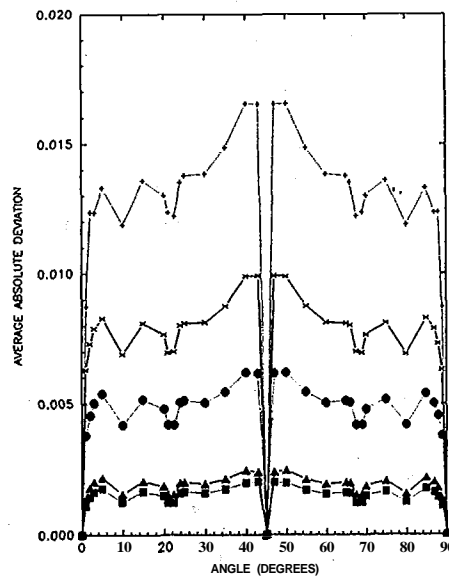


FIGURE 5. GLOBAL ERROR (SINGLE PRECISION) VERSUS ANGLE FOR HEART SCHEME, 5+5. ABSORPTION CO-EFFICIENT = 0.
 • 25 X 25 GRID; x 50 X 50 GRID; • 100 X 100 GRID;
 A 500 X 500 GRID; • 750 X 750 GRID.

The global error using 5+5 channels has a smaller variation and a maximum from 40 to 50 degrees. This maximum is due to the mismatch between entering and leaving faces of the channels.

Comparison of the two sets of figures shows that the HEART scheme yields a global error that can only be reached using Fiveland's method on a large grid. For example, the global error for HEART on a 25 X 25 grid using 5+5 channels is equivalent to Fiveland's scheme on a 500 X 500 grid. The error for Fiveland's method on a 1000 X 1000 grid can be reached using the HEART scheme on a 50 X 50 grid using 5+5 channels.

The advantage of HEART is that it can yield a global error on a coarse grid that can only be matched by central differencing using very large grids. It is non-oscillatory and guarantees non-negative intensities.

The T_N Quadrature Sets

The T_N quadrature sets are the two-dimensional equivalent of the rectangle rule used in one-dimensional integration. The surface of the unit sphere is subdivided into non-overlapping regions. A ray is associated with each region and falls within the solid angle defined by the region. The intensity along the ray is considered representative of the region. Angular integrals are estimated as the sum over all regions of the product of the intensity and the area of the region.

In the T_N quadrature sets, the subdivision of the unit sphere satisfies the rotation/reflection symmetries detailed by Lathrop and Carlson (1968). These symmetries must be respected so that the estimates of angular integrals are independent of the labelling of the co-ordinate axes. If the symmetries are not respected, then it is impossible to distinguish between numerical error and the bias induced by labelling of co-ordinate axes.

The derivation of the T_N quadrature set is accomplished in three steps. First, the octant is projected onto the equilateral triangle defined by the three points (1,0,0), (0,1,0) and (0,0,1). This equilateral triangle is called the basal triangle. The basal triangle is then tessellated with smaller equilateral triangles. This results in the basal triangle being covered with N^2 smaller equilateral triangles, where $N = 1, 2, 3, \dots$. The length of a side of a smaller triangle is $1/N$ the length of a side of the basal triangle. The ray associated with each triangle is defined to pass through the centroid of the triangle. The final step is the projection of the assembly of vertices and centroids onto the surface of the unit sphere. This yields the subdivision of the octant and the direction associated with each region. The weight used in the quadrature set is the area of the region. The total number of rays over the unit sphere is $8N^2$ or N^2 per octant.

The projection used to map the octant onto the basal triangle is accomplished in two steps. A point on the sphere is connected to the origin by a line. The intersection of the line with the basal triangle defines the projected point on the basal triangle.

Comparison to Benchmark Calculations.

Two problems are used to benchmark the numerical calculations. The first problem is a rectangle enclosure containing a hot gas which has an emittance of one. The walls of the enclosure are grey and assumed to have zero emittance. The heat flux to the wall is presented graphically by Raithby and Chui

(1989) and Thynell and Lin (1989). The second problem is a rectangular enclosure with one hot wall that has an emittance of one. The remaining walls have zero emittance. All walls are black. The grey gas is in radiative equilibrium with the hot wall. There are four quantities available for comparison: heat flux to the top (hot), side, bottom walls and the source along the vertical centreline. These are tabulated in Crosbie and Schrenker (1984).

Figure 6 shows the predicted and exact heat flux to the wall for the first problem using Fiveland's method and the standard quadrature sets. The computation was carried out on a 31 X

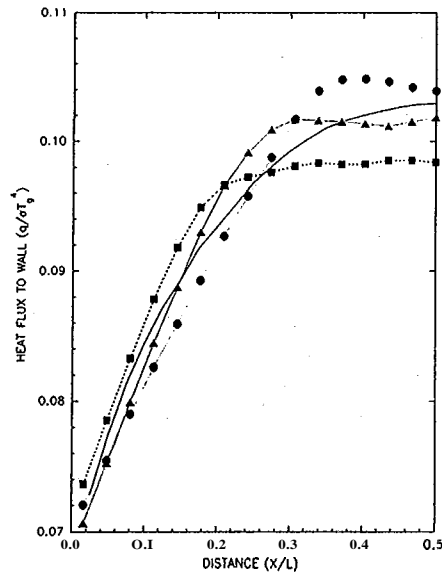


FIGURE 6. HEAT FLUX IN A 1 X 1 DUCT WITH UNIFORM GAS TEMPERATURE. COMPUTED USING FIVELAND'S SCHEME ON A 31 X 31 GRID, $K = 0.1$, AND VARIED QUADRATURE. — EXACT, RAITHYBY & CHUI (1989), FIG. 6. $\bullet S_4$; $\blacktriangle S_5$; $\blacksquare S_6$.

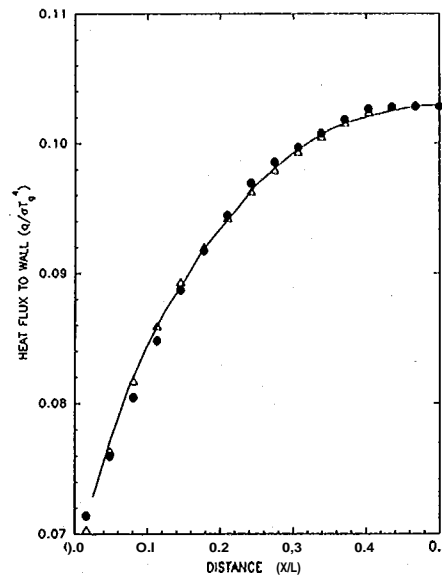


FIGURE 7. HEAT FLUX IN A 1 X 1 DUCT WITH UNIFORM GAS TEMPERATURE. COMPUTED USING HEART SCHEME, 5+5 ON A 31 X 31 GRID, $K = 0.1$, AND VARIED QUADRATURE. — EXACT, RAITHYBY & CHUI (1989), FIG. 8. $\bullet T_4$; $\blacktriangle T_6$.

31 grid with an absorption co-efficient of 0.1; using a 241 X 241 grid caused only minor changes to the numerical results. The numerical solution progressively diverges from the exact solution in the region from 0.35 to 0.50 as the order of the quadrature is increased.

Figure 7 shows the same calculation using HEART with T_3 and T_6 quadrature sets. The computation was carried out on a 31 X 31 coarse grid with 5+5 channels. Satisfactory agreement is achieved between exact and numerical solution. Decreasing the number of channels (to 1+1) yielded the same numerical solution.

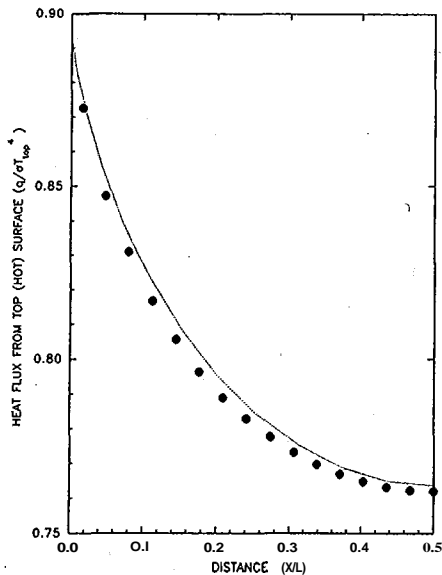


FIGURE 8a. GAS IN RADIATIVE EQUILIBRIUM IN A 1 X 1 DUCT. HEAT FLUX FROM THE TOP (HOT) SURFACE. $K = 1$. — EXACT. CROSBIE & SCHRENKER (1984), TABLE 4. • FIVELAND'S SCHEME, 31 X 31 GRID AND S_8 .

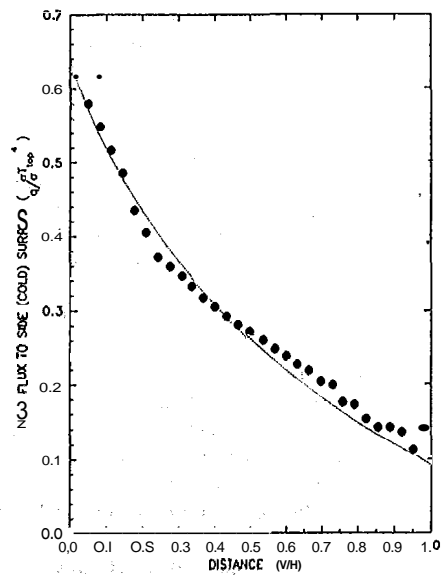


FIGURE 8b. GAS IN RADIATIVE EQUILIBRIUM IN A 1 X 1 DUCT. HEAT FLUX TO THE SIDE (COLD) SURFACE. $K = 1$. — EXACT. CROSBIE & SCHRENKER (1984), TABLE 4. • FIVELAND'S SCHEME, 31 X 31 GRID AND S_6 .

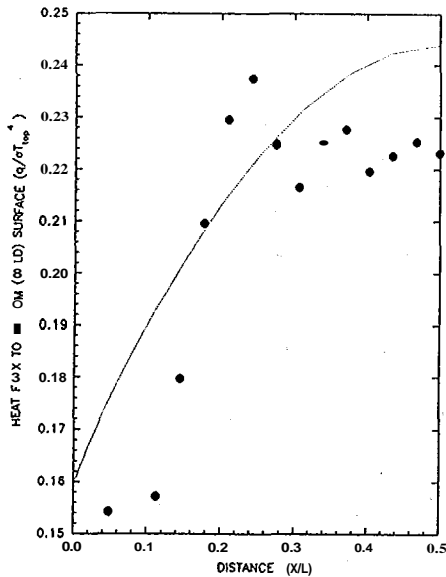


FIGURE 8c. GAS IN RADIATIVE EQUILIBRIUM IN A 1 X 1 DUCT. HEAT FLUX TO THE BOTTOM (COLD) SURFACE. $K = 1$. — EXACT. CROSBIE & SCHRENKER (1984), TABLE 4. • FIVELAND'S SCHEME, 31 X 31 GRID AND S_6 .

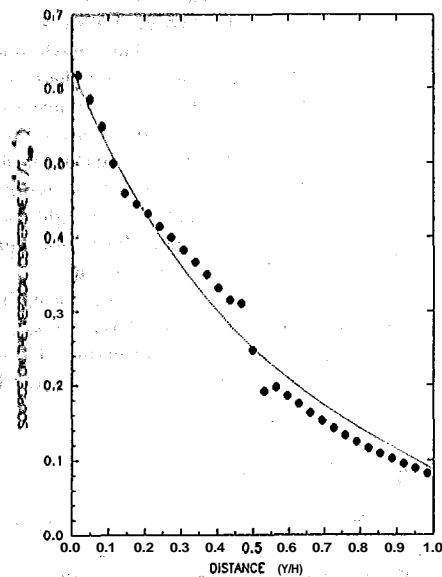


FIGURE 8d. GAS IN RADIATIVE EQUILIBRIUM IN A 1 X 1 DUCT. SOURCE ON THE VERTICAL CENTERLINE. $K = 1$. — EXACT. CROSBIE & SCHRENKER (1984), TABLE 4. • FIVELAND'S SCHEME, 31 X 31 GRID AND S_6 .

Figures 8(a) to 8(d) compare numerical results to benchmark (exact) calculations for the second problem using S_8 quadrature and Fiveland's method using a 31 X 31 grid. The combination fails to predict the bottom heat flux and there are discrepancies in the prediction of heat flux to the side and top wall. The source on the vertical centreline is poorly predicted.

Next, the HEART scheme is used to compute the intensity field. The grid is kept fixed at 31 X 31 control volumes and a HEART, 5+5 scheme is used with the S_8 quadrature set. Only the heat flux to the bottom surface is presented in figure 9. Only a marginal improvement is seen.

The second attempt at improvement reverts to using Fiveland's scheme with the T_6 quadrature sets. A 31 X 31 grid is used. Better agreement between benchmark and numerical is obtained for the bottom heat flux (figure 10) using a T_6 quadrature set.

Figures 11(a) to 11(d) compare numerical and benchmark results for the HEART, 5+5 scheme on a 31 X 31 coarse grid with T_6 quadrature. Satisfactory agreement is obtained between numerical and benchmark calculations for the heat flux to the top and side wall and for the source along the vertical centreline. The predicted heat flux to the bottom wall is in adequate agreement with benchmark results. Comparison to Fiveland's scheme and T_6 quadrature shows that use of HEART secures much better agreement between benchmark and numerical results for all quantities.

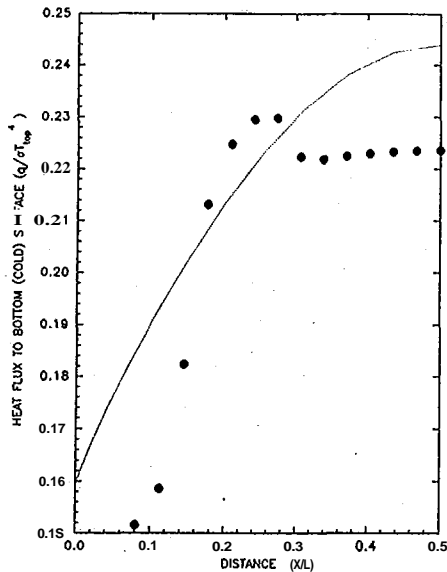


FIGURE 9. GAS IN RADIATIVE EQUILIBRIUM IN A 1 X 1 DUCT. HEAT FLUX TO THE BOTTOM (COLD) SURFACE. $K = 1$.
 — EXACT. CROSSBIE & SCHRENKER (1984), TABLE 4.
 • HEART SCHEME, 5+5, 31 X 31 GRID AND S_2 .

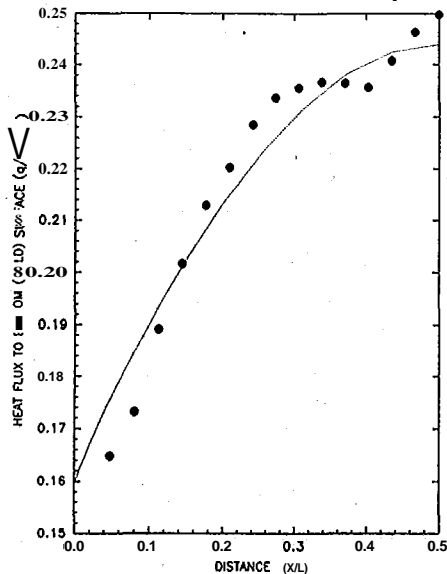


FIGURE 10. GAS IN RADIATIVE EQUILIBRIUM IN A 1 X 1 DUCT. HEAT FLUX TO THE BOTTOM (COLD) SURFACE. $K = 1$.
 — EXACT. CROSSBIE & SCHRENKER (1984), TABLE 4.
 • FIVELAND'S SCHEME, 31 X 31 GRID AND T_6 .

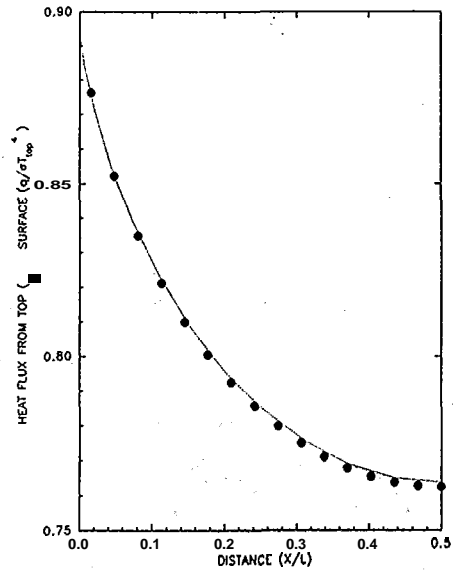


FIGURE 11a. GAS IN RADIATIVE EQUILIBRIUM IN A 1 X 1 DUCT. HEAT FLUX FROM THE TOP (HOT) SURFACE. $K = 1$.
 — EXACT. CROSSBIE & SCHRENKER (1984), TABLE 4.
 • HEART SCHEME, 5+5, 31 X 31 GRID AND T_6 .

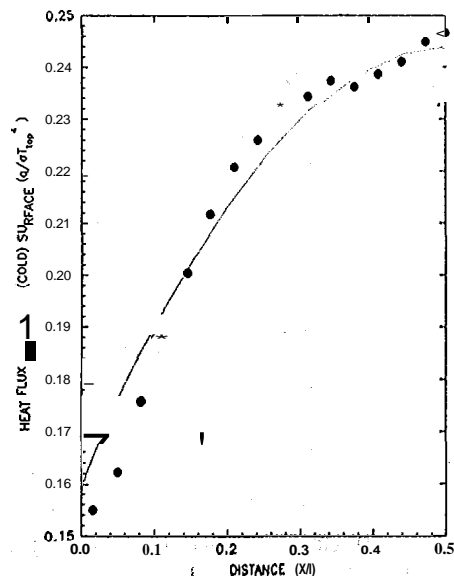


FIGURE 11b. GAS IN RADIATIVE EQUILIBRIUM IN A 1 X 1 DUCT. HEAT FLUX TO THE BOTTOM (COLD) SURFACE. $K = 1$.
 — EXACT. CROSSBIE & SCHRENKER (1984), TABLE 4.
 • HEART SCHEME, 5+5, 31 X 31 GRID AND T_6 .

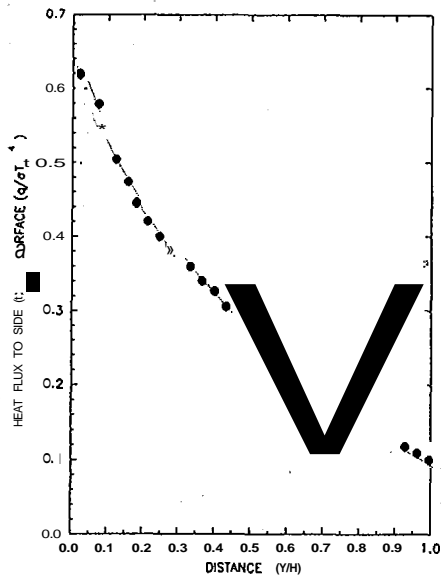


FIGURE 11c. GAS IN RADIATIVE EQUILIBRIUM IN A 1 X 1 DUCT. HEAT FLUX TO THE SIDE (COLD) SURFACE. $K = 1$.
 — EXACT. CROSBIE & SCHRENKER (1984), TABLE 4.
 • HEART SCHEME, 5+5, 31 X 31 GRID AND T_e .

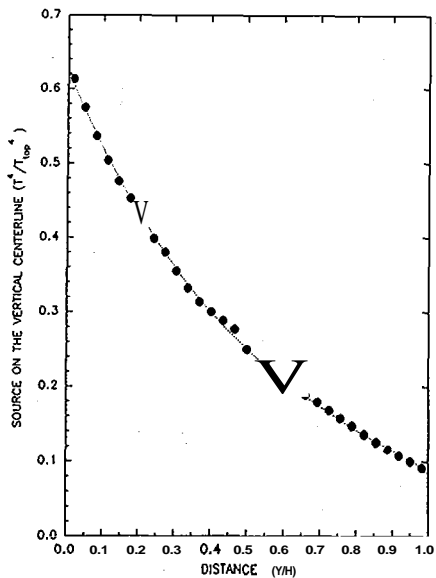


FIGURE 11d. GAS IN RADIATIVE EQUILIBRIUM IN A 1 X 1 DUCT. SOURCE ON THE VERTICAL CENTERLINE. $K = 1$.
 — EXACT. CROSBIE & SCHRENKER (1984), TABLE 4.
 • HEART SCHEME, 5+5, 31 X 31 GRID AND T_e .

Conclusion

Comparison of the HEART scheme and Fiveland's method for solving the equation of transfer showed:

1. the HEART yields non-oscillatory intensity field
2. the intensity is non-negative
3. central differencing requires a large grid to yield an accurate solution to the equation of transfer. The HEART scheme can yield an accurate solution on a smaller grid.

A new family of quadrature sets (T_N) is presented that can be extended to indefinite number of directions.

The combination of HEART and T_N quadrature provides numerical results that are superior to the common solution technique of central differencing and S_n quadrature.

Acknowledgements

The financial support of the Natural Science and Engineering Research Council of Canada, the Ministry of Energy of Ontario and the Ferrous Industry Energy Research Association is gratefully acknowledged.

References

- Crosbie, A.L. and Schrenker, R.G. (1984): J. Quant. Spectrosc. Radiat. Transfer, Vol. 31, No. 4, pp. 339-372.
- Fiveland, W.A. (1984): J. Heat Transfer, Vol. 106, pp. 699-706.
- Fiveland, W.A. (1988): J. Thermophysics, Vol. 2, No. 4, pp. 309-316.
- Hottel, H.C. and Sarofim, A.F. (1967): Radiative Transfer, McGraw Hill.
- Hyde, D.J. and Truelove, J.S. (1977): HTFS RS 189: The Discrete Ordinates Approximation for Multidimensional Radiant Heat Transfer in Furnaces, AERE-R8502, A.E.R.E. Harwell.
- Jamaluddin, A.S. and Smith, P.J. (1988): Combust. Sci. and Tech., Vol. 59, pp. 321-340.
- Larsen, E.W. (1982): Nucl. Sci. Engng., Vol. 80, pp. 710-713
- Lathrop, K.D. (1969): J. Comput. Phys., Vol. 4, pp. 475-498
- Lathrop, K.D. and Carlson, B.G. (1968): Transport Theory. The Method of Discrete Ordinates in Computing Methods in Reactor Physics, Eds. Greenspan, Kelber, Okrent, Gordon and Breech.
- Lockwood, F.C. and Shah, N.G. (1978): Sixth International Heat Transfer Conference 1978, Vol. 2, pp. 33-41.
- Raithby, G.D. and Chui, E.H. (1989): Heat Transfer Phenomena in Radiation, Combustion and Fires, HTD-Vol. 106, 1989 National Heat Transfer Conference, ASME.
- Selcuk, N. (1985): J Heat Transfer, Vol. 107, pp. 648-655.
- Selcuk, N. (1988): Int. J. Heat Mass Transfer, Vol. 31, No. 7, pp. 1477-1482.
- Siddall, R.G. and Selcuk, N. (1979): Trans. I. Chem. E., Vol. 57, pp. 163-169.
- Thynell, S.T. and Lin, W.-Q. (1989) Heat Transfer Phenomena in Radiation, Combustion and Fires, HTD-Vol. 106, 1989 National Heat Transfer Conference, ASME.
- Truelove, J.S. (1987): J Heat Transfer, Vol. 109, pp. 1048-1051.
- Truelove, J.S. (1988): J. Quant. Spectrosc. Radiat. Transfer, Vol. 39, No. 1, pp. 27-31.
- Viskanta, R. and Menguc, M.P. (1987): Prog. Energy Combust. Sci., Vol. 13, pp. 97-160.